Localized surface-plasmon resonances on single and coupled nanoparticles through surface integral equations for flexible surfaces

Rogelio Rodríguez-Oliveros* and José A. Sánchez-Gil

Instituto de Estructura de la Materia, Consejo Superior de Investigaciones Científicas, Serrano 121, 28006 Madrid, Spain

**rogelio@iem.cfmac.csic.es*

Abstract: We present an advanced numerical formulation to calculate the optical properties of 3D nanoparticles (single or coupled) of arbitrary shape and lack of symmetry. The method is based on the (formally exact) surface integral equation formulation, implemented for parametric surfaces describing particles with arbitrary shape through a unified treatment (Gielis' formula). Extinction, scattering, and absorption spectra of a variety of metal nanoparticles are shown, thus determining rigorously the localised surface-plasmon resonances of nanocubes, nanostars, and nanodimers. Far-field and near-field patterns for such resonances are also calculated, revealing their nature. The flexibility and reliability of the formulation makes it specially suitable for complex scattering problems in Nano-Optics & Plasmonics.

OCIS codes: (240.6680) Surface plasmons; (290.5850) Scattering, particles; (250.5403) Plasmonics.

References and links

1. X. Lu, M. Rycenga, S. E. Skrabalak, B. Wiley, and Y. Xia, "Chemical synthesis of novel plasmonic nanoparticles," Annu. Rev. Phys. Chem. **60**, 167–92 (2009).
2. T. R. Jensen, G. C. Schatz, and R. P. V. Duyne, "Nanosphere lithography: surface plasmon resonance spectrum of a periodic array of silver nanoparticles by ultraviolet-visible extinction spectroscopy and electrodynamic modeling," J. Phys. Chem. B **103**, 2394–2401 (1999).
3. A. Ono, J. Kato, and S. Kawata, "Subwavelength optical imaging through a metallic nanorod array," Phys. Rev. Lett. **95**, 267407 (2005).
4. E. Ozbay, "Plasmonics: merging photonics and electronics at nanoscale dimensions," Science **311**, 189–193 (2006).
5. V. Giannini, A. Fernandez-Dominguez, Y. Sonnefraud, T. Roschuk, R. Fernandez-García, and S. A. Maier, "Controlling light localization and light–matter interactions with nanoplasmonics," Small **6**, 2498–2507 (2010).
6. L. Novotny and N. van Hulst, "Antennas for light," Nat. Photonics **5**, 83–90 (2011).
7. J. A. Sánchez-Gil and J. V. García-Ramos, "Local and average electromagnetic enhancement in surface-enhanced Raman scattering from self-affine fractal metal substrates with nanoscale irregularities," Chem. Phys. Lett. **367**, 361–366 (2003).
8. E. J. Zeman and G. C. Schatz, "An accurate electromagnetic theory study of surface enhancement factors for Ag, Au, Cu, Li, Na, Al, Ga, In, Zn, and Cd," J. Phys. C **91**, 634–643 (1987).
9. H. Xu, J. Aizpurua, M. Käll, and P. Apell, "Electromagnetic contributions to single-molecule sensitivity in surface- enhanced Raman scattering," Phys. Rev. E **62**, 4318–4324 (2000).
10. P. Mühlschlegel, H. J. Eisler, O. J. F. Martin, and B. Hecht, "Resonant optical antennas," Science **308**, 1607–1609 (2005).

#144976 - $15.00 USD Received 29 Mar 2011; revised 19 May 2011; accepted 22 May 2011; published 8 Jun 2011

11. J. J. Greffet, "Nanoantennas for light emission," Science **308**, 1561–1563 (2005).
12. O. L. Muskens, V. Giannini, J. A. Sánchez-Gil, and J. Gómez Rivas, "Strong enhancement of the radiative decay rate of emitters by single plasmonic nanoantennas," Nano Lett. **7**, 2871–2875 (2007).
13. T. H. Taminiau, R. J. Moerland, F. B. Segerink, L. Kuipers, and N. F. V. Hulst, "$\lambda/4$ resonance of an optical monopole antenna probed by single molecule fluorescence," Nano Lett. **7**, 28–33 (2007).
14. C. Bohren and D. Huffman, *Absorption and Scattering of Light by Small Particles* (Wiley, 1998).
15. W. L. Barnes, "Comparing experiment and theory in plasmonics," J. Opt. A, Pure Appl. Opt. **11**, 114002 (2009).
16. K. S.Yee, "Numerical Solution of initial value problems of Maxwells equations," IEEE Trans. Antenn. Propag. **14**, 302–307 (1966).
17. R. Clough, "The finite element method after twenty-five years: a personal view," Comput. Struct. **12**, 361–370 (1980).
18. C. Girard and A. Dereux, "Near-field optics theories," Rep. Progr. Phys. **59**, 657 (1996).
19. B. T. Draine and P. J. Flatau, "Discrete-Dipole approximation for scattering calculations," J. Opt. Soc. Am. A **11**, 1491 (1994).
20. M. I. Mishchenko, N. T. Zakharova, G. Videen, N. G. Khlebtsov, and T. Wriedt, "Comprehensive T-matrix reference database: a 2007–2009 update," J. Quant. Spectrosc. Radiat. Tranfer. **111**, 650–658 (2010).
21. V. Myroshnychenko, E. Carbó-Argibay, I. Pastoriza-Santos, J. Pérez-Juste, L. M. Liz-Marzán, and F. García de Abajo, "Modeling the optical response of highly faceted metal nanoparticles with a fully 3D boundary element method," Adv. Mater. **20**, 4288–4293 (2008).
22. A. A. Maradudin, T. R. Michel, A. Mcgurn, and E. R. Mendez, "Enhanced backscattering of light from a random grating," Ann. Phys. **203**, 255–307 (1990).
23. J. A. Sanchez-Gil and M. Nieto-Vesperinas, "Light scattering from random rough dielectric surfaces," J. Opt. Soc. Am A **8**, 1270 (1991).
24. S. Rao, D. Wilton, and A. Glisson, "Electromagnetic scattering by surfaces of arbitrary shape," IEEE Trans. Antenn. Propag. **30**, 409–418 (1982).
25. A. M. Kern and O. J. F. Martin, "Surface integral formulation for 3D simulations of plasmonics and high permittivity nanostructures," J. Opt. Soc. Am. A **26**, 732–740 (2009).
26. P. Tran and A. Maradudin, "The scattering of electromagnetic waves from two-dimensional randomly rough perfectly conducting surfaces: the full angular intensity distribution," Opt. Commun. **110**, 269–273 (1994).
27. K. Pak, L. Tsang, and J. Johnson, "Numerical simulations and backscattering enhancement of electromagnetic waves from two-dimensional dielectric random rough surfaces with the sparse-matrix canonical grid method," J. Opt. Soc. Am. A **14**, 1515 (1997).
28. I. Simonsen, A. A. Maradudin, and T. A. Leskova, "The scattering of electromagnetic waves from two-dimensional randomly rough perfectly conducting surfaces: the full angular intensity distribution," Phys. Rev. A **81**, 013,806 (2009).
29. I. Simonsen, A. A. Maradudin, and T. A. Leskova, "Scattering of Electromagnetic Waves from Two-Dimensional Randomly Rough Penetrable Surfaces," Phys. Rev. Lett. **104**, 223,904 (2010).
30. C. I. Valencia, E. R. Méndez, B. S. Mendoza, "Second-harmonic generation in the scattering of light by two dimensional nanoparticles," J. Opt. Soc. Am. B **20**, 2150–2161 (2003).
31. V. Giannini and J. A. Sánchez-Gil, "Calculations of light scattering from isolated and interacting metallic nanowires of arbitrary cross section by means of Green's theorem surface integral equations in parametric form," J. Opt. Soc. Am. A **24**, 2822 (2007).
32. U. Hohenester and J. Krenn, "Surface plasmon resonances of single and coupled metallic nanoparticles: a boundary integral method approach," Phys. Rev. B **72**, 1–9 (2005).
33. J. Jung and T. Sodergaard, "Greens function surface integral equation method for theoretical analysis of scatterers close to a metal interface," Phys. Rev. B **77**, 245310 (2008).
34. P. I. Geshev, U. Fischer, and H. Fuchs, "Calculation of tip enhanced Raman scattering caused by nanoparticle plasmons acting on a molecule placed near a metallic film," Phys. Rev. B **81**, 125,441 (2010).
35. J. Gielis, "A generic geometric transformation that unifies a wide range of natural and abstract shapes," Am. J. Bot. **90**, 333–338 (2003).
36. J. Stratton and L. Chu, "Diffraction theory of electromagnetic waves," Phys. Rev. **56**, 99–107 (1939).
37. M. Born and E. Wolf, *Principles of Optics*, 6th ed. (Pergamon, 1980).
38. H. Ying Yao and Y. Bing Gan, "Regularization of the combined field integral equation on parametric surface for EM scattering problems," Electromagnetics **26**, 423–438 (2006).
39. P. Bourke, "SuperShape in 3D," URL `http://local.wasp.uwa.edu.au/~{}pbourke/geometry/supershape3d/`.
40. H. Van De Hulst, *Light Scattering by Small Particles*, 1st ed. (Dover, 1981).
41. P. B. Johnson and R. W. Christie, "Optical constants of nobel metals," Phys. Rev. B **6**, 4370 (1972).
42. S. Y. Lee, L. Hung, G. S. Lang, J. E. Cornett, I. D. Mayergoyz, and O. Rabin, "Dispersion in the SERS enhancement with silver nanocube dimers," ACS Nano **4**, 5763–5772 (2010).
43. A. L. González and C. Noguez, "Optical properties of silver nanoparticles," Phys. Stat. Solidi C **4**, 4118–4126 (2007).

#144976 - $15.00 USD Received 29 Mar 2011; revised 19 May 2011; accepted 22 May 2011; published 8 Jun 2011

44. V. Giannini, R. Rodríguez-Oliveros, and J. A. Sánchez-Gil, "Surface plasmon resonances of metallic nanostars/nanoflowers for surface-enhanced raman scattering," Plasmonics **5**, 99–104 (2010).
45. P. Senthil Kumar, I. Pastoriza-Santos, B. Rodríguez-González, F. Javier García de Abajo, and L. M. Liz-Marzán, "High-yield synthesis and optical response of gold nanostars," Nanotechnology **19**, 015606 (2008).
46. E. R. Encina and E. A. Coronado, "Plasmon coupling in silver nanosphere pairs," J Chem. Phys. C **114**, 3918–3923 (2010).
47. A. García-Etxarri, R. Gómez-Medina, L. S. Froufe-Pérez, C. López, L. Chantada, F. Scheffold, J. Aizpurua, M. Nieto-Vesperinas, and J. J.Sáenz, "Strong magnetic response of Silicon nanoparticles in the infrared," Opt. Express **19**, 4815–4826 (2011).

1. Introduction

In the last decades, nanofabrication and detection techniques have achieved a remarkable development providing the tools to fabricate and characterise particles at the nanoscale in many different shapes and materials [1–3]. Nanoparticles have been key to the intensive research on Plasmonics [4–6], since these nanoparticles may exhibit localised surface plasmon resonances (LSPRs), the collective oscillations of the sea of electrons on the surface of the nanoparticles. One of the most appealing features of LSPRs is the huge amplification of the electromagnetic field (EM) at the resonance wavelengths, that have been widely applied in spectroscopy and more explicitly on surface-enhanced Raman spectroscopy (SERS) [7–9]. Moreover, their ability to strongly couple light in and out as nanoantennas has widely been stressed lately [5, 10–13].

From the theoretical point of view, a big effort has been recently focused on revisiting and developing methods to solve (Maxwell) scattering equations. A few analytical solutions are known for very simple geometrical shapes as spheres, cylinders or ellipsoids [14]. As long as the interest typically lies in nanoparticles with complex, arbitrary shapes, or interacting particles, a numerical approach is usually needed [15].

A wide range of methods are available for studying optical scattering problems in the classical regime, which can be roughly classified according to: (i) Volume methods (integral and differential) as the finite-different time domain (FDTD) [16] and finite element method (FEM) [17], where the whole space has to be discretized in order to calculate the electromagnetic field, and dyadic green function technique [18], and Discrete Dipole Approximation (DDA) [2, 19], where the scatterer volume has to be discretized; and (ii) surface methods as the T-Matrix [20], boundary element method (BEM) [21], and various implementations of surface integral equations (SIE) [22, 23], where only the surface of the scatterers has to be discretized, saving computational time and memory requirements. Incidentally, their reliability has been recently revised, and questioned, with regard to the simple validity criterion of reproducing the LSPR of a metal nanosphere [15].

There exist different implementations of the SIE based on the vectorial version of the second Green's theorem. In this regard, commonly used in the microwave regime is the method of moments (MoM) [24], which has recently been extended to the visible [25]. On the other hand, the Green's theorem method (GTm) became an appealing method in the early nineties to study 2D semi-infinite rough surfaces [22]. The GTm has been implemented in many different ways, for many different geometrical configurations: 1D semi-infinite rough surfaces [22, 23], 2D semi-infinite rough surfaces [26–29], 2D closed surfaces in parametric equations [30, 31], 3D closed surfaces in electrostatic approximation [32, 33], and 3D closed surfaces with axial symmetry [34]. However, it remains still undone a general implementation of the GTm for 3D closed surfaces without any approximation.

In this article we introduce a general formulation of the GTm for an arbitrary number of 3D-scatterers with arbitrary shape, with the help of what we call flexible surfaces: From a unique formula in parametric coordinates, the 3D extension of 2D Gielis' superformula [35], a variety of shapes can be implemented by only modifying the shape parameters. This allows us to obtain

#144976 - $15.00 USD Received 29 Mar 2011; revised 19 May 2011; accepted 22 May 2011; published 8 Jun 2011

scattering, extinction, and absorption spectra, along with near field distributions and radiation patterns at given wavelengths, for nontrivial geometries of undoubtedly interest in Plasmonics and Nanophotonics. This work is organised as follows. In Section 2, we introduce the scattering equations for one and more scatterers in terms of the components of the electromagnetic field on the surface, and the numerical implementation of the method. In Section 3, we discuss useful expressions to describe surfaces called flexible surfaces. Next in Section 4, we show how the method works including results of LSPRs for a variety of complex nanoparticles: spheres (to test Mie), cubes, dimers and stars. We finally draw conclusions from the results in Section 5.

2. General description of the method

2.1. Scattering equations for a single scatterer

In Fig. 1, we show the physical configuration of the scattering problem we are dealing with: A group of scatterers made of different materials with arbitrary shape embedded in a surrounding medium characterised by a dielectric permittivity ε_{out}. A monochromatic plane wave of frequency ω (incident field), impinges on the scatterers with module $|\mathbf{E}_i|$ at an arbitrary direction of propagation with propagation constant $k_0 = \frac{\omega}{c}\sqrt{\varepsilon_{out}}$. It is assumed all over the paper that the time dependence of the fields is harmonic $e^{-i\omega t}$. The electromagnetic fields outside $(\mathbf{E}^{>},\mathbf{H}^{>})$, and inside $(\mathbf{E}^{<},\mathbf{H}^{<})$ of a scatterer with volume V and arbitrary shape Ω generated by the interaction between the scatterer and the incident field are described by the Stratton-Chu equations [26, 27, 36]:

$$\mathbf{E}^{>}(\mathbf{r}) = \mathbf{E}^{inc}(\mathbf{r}) - \frac{1}{4\pi}\int ik\mu G_0(\mathbf{r},\mathbf{r}')(\mathbf{n}'\times\mathbf{H}^{>}(\mathbf{r}'))dS' + \frac{1}{4\pi}\int(\mathbf{n}'\times\mathbf{E}^{>}(\mathbf{r}'))\times\nabla' G_0(\mathbf{r},\mathbf{r}') + (\mathbf{n}'\cdot\mathbf{E}^{>}(\mathbf{r}'))\nabla' G_0(\mathbf{r},\mathbf{r}')dS', \quad r\notin V, \tag{1a}$$

$$\mathbf{E}^{<}(\mathbf{r}) = -\frac{1}{4\pi}\int ik\mu G_\varepsilon(\mathbf{r},\mathbf{r}')(\mathbf{n}'\times\mathbf{H}^{<}(\mathbf{r}'))dS' - \frac{1}{4\pi}\int(\mathbf{n}'\times\mathbf{E}^{<}(\mathbf{r}'))\times\nabla' G_\varepsilon(\mathbf{r},\mathbf{r}') + \frac{\varepsilon_{out}}{\varepsilon_{in}}(\mathbf{n}'\cdot\mathbf{E}^{<}(\mathbf{r}'))\nabla' G_\varepsilon(\mathbf{r},\mathbf{r}')dS', \quad r\in V, \tag{1b}$$

$$\mathbf{H}^{>}(\mathbf{r}) = \mathbf{H}^{inc}(\mathbf{r}) - \frac{1}{4\pi}\int ikG_0(\mathbf{r},\mathbf{r}')(\mathbf{n}'\times\mathbf{E}^{<}(\mathbf{r}'))dS' + \frac{1}{4\pi}\int(\mathbf{n}'\times\mathbf{H}^{<}(\mathbf{r}'))\times\nabla' G_0(\mathbf{r},\mathbf{r}') + (\mathbf{n}'\cdot\mathbf{H}^{<}(\mathbf{r}'))\nabla' G_0(\mathbf{r},\mathbf{r}')dS', \quad r\notin V, \tag{1c}$$

$$\mathbf{H}^{<}(\mathbf{r}) = \frac{1}{4\pi}\int ik\varepsilon_{in} G_\varepsilon(\mathbf{r},\mathbf{r}')(\mathbf{n}'\times\mathbf{E}^{<}(\mathbf{r}'))dS' - \frac{1}{4\pi}\int(\mathbf{n}'\times\mathbf{H}^{<}(\mathbf{r}'))\times\nabla' G_\varepsilon(\mathbf{r},\mathbf{r}') + (\mathbf{n}'\cdot\mathbf{H}^{<}(\mathbf{r}'))\nabla' G_\varepsilon(\mathbf{r},\mathbf{r}')dS', \quad r\in V; \tag{1d}$$

where $G_{\varepsilon/0} = \frac{e^{ik_{in/0}|\mathbf{r}-\mathbf{r}'|}}{|\mathbf{r}-\mathbf{r}'|}$ is the scalar green function in the material with electric permittivity $\varepsilon_{in/out}$, and the vector $\mathbf{n}$ is the normal vector to the surface pointing outwards. In Eqs. (1), we assume $\mu = \mu_{in} = \mu_{out} = 1$.

Equations (1) express the EM fields in the entire space in terms of integrals over the scatterer surface, where the unknown magnitudes are related to the EM fields evaluated on the surface, which play the role of surface EM sources.

2.2. System of integral equations: Surface EM fields

In order to solve Eqs. (1) we have to make two different choices. Firstly, we have to explicitly choose the surface magnitudes that are unknowns in the system of integral equations. In the

#144976 - $15.00 USD Received 29 Mar 2011; revised 19 May 2011; accepted 22 May 2011; published 8 Jun 2011

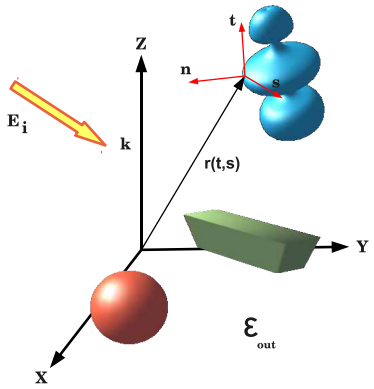

Fig. 1. Schematic representation of the scattering problem. An incident electromagnetic field $\mathbf{E}_i$ impinges on a set of scatterers made of different materials embedded on a medium with permittivity ε_{out}. The vector $\mathbf{r}(t,s)$ is the position vector and $\mathbf{n},\mathbf{t},\mathbf{s}$ denote the local basis on the surface of the scatterers.

literature, sources are chosen with different criteria [26-30]. In this work our unknown surface magnitudes are the (two) tangential and (one) normal components of the surface electromagnetic field, namely:

$$\mathbf{n}\cdot\mathbf{E}^{>}(\mathbf{r}),\mathbf{n}\times\mathbf{E}^{>}(\mathbf{r}),\mathbf{n}\cdot\mathbf{H}^{>}(\mathbf{r}),\mathbf{n}\times\mathbf{H}^{>}(\mathbf{r}). \tag{2}$$

Now we need at least 6 scalar equations from Eqs. (1) to match the 6 unknowns. To this end, we first evaluate Eqs. (1) on the scatterer surface (by making $\mathbf{r}$ tend to Ω from either outside or inside, as needed), and connect EM fields outside and inside through the continuity conditions across the scatterer surface, namely:

$$\varepsilon_{out}\mathbf{n}\cdot\mathbf{E}^{>}=\varepsilon_{in}\mathbf{n}\cdot\mathbf{E}^{<},\mathbf{n}\times\mathbf{E}^{>}=\mathbf{n}\times\mathbf{E}^{<},\mathbf{n}\cdot\mathbf{H}^{>}=\mathbf{n}\cdot\mathbf{H}^{<},\mathbf{n}\times\mathbf{H}^{>}=\mathbf{n}\times\mathbf{H}^{<}. \tag{3}$$

Finally, we choose Eqs (1a,d) (projected to the surface normal) and Eqs (1b,d) (projected to the surface tangents) as the six scalar equations that constitute our system of surface integral equations.

At this point, the local vectorial basis has to be chosen on any point of the surfaces where the sources are going to be calculated. In our 3D-GTm formulation, we choose the two tangent vectors and the normal vector to the surface on any point of the surface scatterer as the vectorial basis:

$$\mathbf{t}\equiv\frac{\mathbf{r}_t}{|\mathbf{r}_t|},\mathbf{s}\equiv\frac{\mathbf{r}_s}{|\mathbf{r}_s|},\mathbf{n}\equiv\frac{\mathbf{r}_t}{|\mathbf{r}_t|}\times\frac{\mathbf{r}_s}{|\mathbf{r}_s|}, \tag{4}$$

where $\mathbf{r}_t$ and $\mathbf{r}_s$ are the derivative of the vector position with respect to the parameters t and s, (see Section 3 below). In this manner, we are explicitly stating the parametric equations as the descriptor of the surfaces, since it is the more natural way to obtain the vectorial basis.

#144976 - $15.00 USD Received 29 Mar 2011; revised 19 May 2011; accepted 22 May 2011; published 8 Jun 2011

2.3. Numerical implementation: Quadrature scheme

In order to convert the above mentioned system of integral equations into a system of linear equations, we introduce a classical quadrature scheme of the surface integrals,

$$\int_S f(S')dS' = \sum_{i=1}^{N} f_{\Delta_i}(r_i), \tag{5}$$

where Δ_i is an arbitrary element of the mesh and r_i denotes the position vector of the point at the centre of the interval. Making use of the quadrature scheme introduced above all over the integrals, and projecting Eqs. (1), as mentioned above, onto the vectors of the natural basis of the surface, Eq. (4), we obtain the system of linear equations. In this regard, we have to take the divergences of the Green function into account. If $r \sim r'$, from the definition of the Green function, it follows that $G(r,r') \to \infty$ and $\nabla G(r,r') \to \infty$. In order to deal with these difficulties, it is needed to perform an analytical integration of the divergences of Eqs. (1) with the prescriptions in Refs. [22, 38]. Roughly speaking, a grid of 10^3 surface elements and a precise integration of the interaction terms involving green function within every interval Δ_i is enough to reach convergence in calculations for isolated particles (e.g. cube) with typical size about 50 nm. The calculation takes nearly 150 minutes on an Intel Xeon Quad-Core X5550 2,67 GHz, without any fine tuning.

2.4. Near field

From the knowledge of the field on the surface and using Eq. (1a) and Eq. (1b), we can calculate the electric near field distribution outside and inside the scatter, respectively. Likewise, Eqs. (1c-d) determine the magnetic near field. Bear in mind that the near EM field components will be described in a vectorial basis (for instance, cartesian or polar coordinates) different from the local vectorial basis onto which the EM fields on the scatterers surface are projected.

2.5. Far field

The starting point to find the expressions ruling the far field distribution are also Eqs. (1a,d), as in the case of the near field. In the far field, $\mathbf{r}' \ll \mathbf{r}$ holds, so that $|\mathbf{r}-\mathbf{r}'| \approx |\mathbf{r}| - \dfrac{\mathbf{r}}{|\mathbf{r}|}\cdot\mathbf{r}'$. Therefore, taking such limit in the general expressions of the Green's function and its gradient leads to:

$$G_0 \approx \frac{e^{ikr}}{r}e^{-i\mathbf{k}\cdot\mathbf{r}'}, \nabla' G_0 \approx -ik\frac{e^{ikr}}{r}e^{-i\mathbf{k}\cdot\mathbf{r}'}. \tag{6}$$

By introducing Eq. (6) into Eq. (1a), we find the expression of the scattered electric field in the far-field, as outgoing spherical waves

$$\begin{aligned}\mathbf{E_{ff}} = \frac{e^{ikr}}{r}\frac{ik}{4\pi}\Bigg[&\int e^{-i\mathbf{k}\cdot\mathbf{r}'}\mathbf{n}'\times\mathbf{H}'dS' - \int e^{-i\mathbf{k}\cdot\mathbf{r}'}(\mathbf{n}'\times\mathbf{E}')\times\mathbf{R}dS' \\ &- \int e^{-i\mathbf{k}\cdot\mathbf{r}'}E'_n\mathbf{R}dS'\Bigg].\end{aligned} \tag{7}$$

Likewise, we can find the equations for the magnetic field.

Equation (7) can be projected onto the polarization plane in the far-field zone, which is defined as the plane perpendicular to the wave number vector $\mathbf{k}$, leading to:

$$\mathbf{E_{fs}} = \frac{e^{ikr}}{r}\frac{ik}{4\pi}\left[\int e^{-i\mathbf{k}\cdot\mathbf{r}'}(\mathbf{n}'\times\mathbf{H}')\cdot\mathbf{R}_s dS' + \int e^{-i\mathbf{k}\cdot\mathbf{r}'}(\mathbf{n}'\times\mathbf{E}')\cdot\mathbf{R}_t\right]dS' \tag{8a}$$

$$\mathbf{E_{ft}} = \frac{e^{ikr}}{r}\frac{ik}{4\pi}\left[\int e^{-i\mathbf{k}\cdot\mathbf{r}'}(\mathbf{n}'\times\mathbf{H}')\cdot\mathbf{R}_t dS' - \int e^{-i\mathbf{k}\cdot\mathbf{r}'}(\mathbf{n}'\times\mathbf{E}')\cdot\mathbf{R}_s\right]dS', \tag{8b}$$

#144976 - $15.00 USD Received 29 Mar 2011; revised 19 May 2011; accepted 22 May 2011; published 8 Jun 2011

where we have used the properties of the mixed product in the second term of Eq. (7). $\mathbf{R}_t$, $\mathbf{R}_s$ are the tangent vectors to the surface of integration in the far field. From the far-field amplitudes, physical magnitudes such as the scattering cross section (Q_{sca}), the extinction cross section (Q_{ext}), and the absorption cross section (Q_{abs}) can be calculated [37]:

$$\begin{aligned} Q_{sc} &= \frac{1}{\sqrt{\varepsilon_o}|\mathbf{E^{inc}}|}\int_{S_{ff}} |\mathbf{E_{ft}}|^2 + |\mathbf{E_{fs}}|^2 dS. \\ Q_{ext} &= \frac{4\pi}{k} Im(\mathbf{E_{ffw}} \cdot \frac{\mathbf{k}_{fw}}{|\mathbf{k}_{fw}|}) \\ Q_{abs} &= Q_{ext} - Q_{sca}. \end{aligned} \tag{9}$$

where fw means the forward direction defined by the direction of incidence.

2.6. Multi-scatterers

Once we have introduced the method, we can generalize it to more than one scatterer. Let M be the number of scatterers, assuming they are not touching each other. The four surface integral equations (Eq. (1)) have to be modified to account for the M scatterers in the following manner. First, those equations describing the electric and magnetic fields in the embedding medium, Eqs. (1a) and (1c), now include the contributions from all M scatterers. Therefore, the two surface integrals in the right-hand sides of Eqs. (1a) and (1c) become 2M integrals over the surface of every scatterer. These 2M surface integrals indeed take into account the interaction between the EM fields from all M scatterers in the surrounding medium. Second, instead of the two equations describing the electric and magnetic fields inside the single scatterer, Eqs. (1b) and (1d), there are 2M equations describing the electric and magnetic fields inside every scatterer. Needless to say, the dielectric functions appearing in the integrands and green functions of each two pair of equations are given by those of the bulk medium of the corresponding scatterer. In this regard, every scatterer can be made of a different material. In summary, we end up with 2+2M surface integral equations to rigorously describe the EM field in the entire space in the case of M scatterers. The details of the numerical implementation will be shown elsewhere.

3. Flexible surfaces: 3D supeshape

We have introduced in the latter section the parametric coordinates as the descriptor of the surface of the scatterers. This could be considered as a limitation of our method, since we need at least a C^1 class function with respect to both parameters in order to achieve the expressions of the parametric equations of the surfaces. For instance, if we wish to consider a cube shape in our method, we should use a piecewise function in order to describe the six faces of the cube, arising indeed problems of sharpness related with the cube vertex. Moreover, the tangent vectors of the vertex would not be well defined.

In order to deal with these kind of problems, we introduce flexible surfaces, namely a surface based on the coordinates of a well known surface such as a sphere, a plane, a torus,.., with the commonly constant parameters of those surfaces depending however on the natural parameters of the surface as well. The flexible surface based on a sphere, called *supershape* (SS) or *superformula* [35, 39], gives rise to a variety of exotic surfaces commonly used in the field of Plasmonics, from a simple sphere to cube, cylinder, cone, tetrahedron, prism, and star. The parameters allow us to change not only the symmetry of the shape but also the sharpness of the

#144976 - $15.00 USD Received 29 Mar 2011; revised 19 May 2011; accepted 22 May 2011; published 8 Jun 2011

vertex, getting closer to realistic nanoparticle designs. The SS parametric equations are:

$$x(t,s) = r_1(s)r_2(t)sin(t)cos(s) \tag{10a}$$

$$y(t,s) = r_1(s)r_2(t)sin(t)sin(s) \tag{10b}$$

$$z(t,s) = r_2(t)cos(t), \tag{10c}$$

where

$$r(u) = \left(\left| \frac{1}{a} sin\left(\frac{m}{4}u\right) \right|^{n_2} + \left| \frac{1}{b} cos\left(\frac{m}{4}u\right) \right|^{n_3} \right)^{-\frac{1}{n_1}}, u = t,s \tag{11}$$

and r_1, r_2 are two different realizations of the parameters n_1, n_2, n_3, m, a, b in Eq. (11).

In order to understand how the supershape works, we can consider the set of Eqs. (10) as a deformation of the spherical coordinates, where the parameters t and s play the role of the angles in spherical coordinates, and the radius depends on them as well. That local dependence of the radius on the angles makes the supershape become different surfaces, for different groups of parameters, $n_1, n_2, ...$ For a catalogue of the different shapes allowed to the spherical supershape and to different supershapes, as the toroidal one, see e.g. Ref. [39].

The parameters t and s are not the natural parameters of the supershape, so that the resulting tangent and normal vectors are not an orthogonal base. Therefore we have to use the Gram-Schmidt orthogonalization process in order to find an orthogonal basis.

4. LSPR on complex nanoparticles

4.1. Single nanospheres: Mie comparison

With the purpose of comparing this method with the exact solution due to Mie [14, 40], we have calculated Q_{sca} and Q_{ext} in vacuum for a metal sphere made of silver [41] with 5 nm radius. In Fig. 2(a,b) we show the dipole LSPR of the sphere at 355 nm calculated with both methods. GTm clearly reproduces the Mie spectra, although the resonance is very sharp, which requires more accuracy from a numerical method [15]. In Fig. 2(c), we show the 3D radiation pattern calculated with our GTm at the LSPR, revealing the expected toroidal pattern with no radiation along the polarization direction (dipolar pattern). In Fig. 2(d) the radiation pattern distribution on both the polarization plane and the perpendicular one is plotted at the resonance wavelength, showing that the dipolar pattern exhibits in fact slightly asymmetrical lobes, as expected. Finally, the near field distribution on the plane of polarization at the LSPR is plotted in Fig. 2(e) corroborating the expected dipolar charge distribution along the polarization direction (x axis). The near field amplitude is shown along the white line drawn in Fig. 2(e) for both the Mie and the GTm solutions, in Fig. 2(f), confirming the accuracy of the GTm also for near field calculations.

4.2. Single supershape: from sharp/rounded nanocubes to nanostars

To reveal the flexibility of our GTm implementation, we now study the dependence of the Q_{sca} of a silver cube in vacuum on the rounded level of the corners. This is indeed a critical issue upon comparing theoretical calculations with experimental measurements, for real life nanoparticles often differ from perfect mathematical shapes [42]. In order to generate a cube with the SS, we have to choose $n_1 = n_2 = n_3 \equiv n > 4$, $a = b = 1$, and $m = 4$. The parameter m and the degeneracy of the parameters n_1, n_2, n_3 to n defines the system as a cube. Taking different values for n, from $n = 5$ to $n = 20$, we change the sharpness of the cube corners, the larger the value of n the sharper corners; for $n > 20$ the cube sharpness does not significantly change. The results are shown in Fig. 3. It is readily observed that, two changes are produced on the Q_{sca} with increasing n. Firstly, if we make the corners sharper the scattering of the cube becomes

#144976 - $15.00 USD Received 29 Mar 2011; revised 19 May 2011; accepted 22 May 2011; published 8 Jun 2011

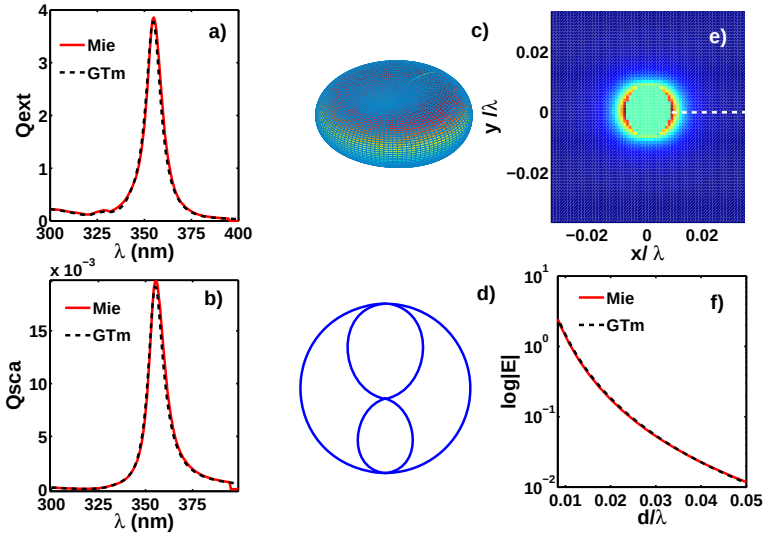

Fig. 2. (a) Qext and (b) Qsca for the GTm (black-dashed curve) and the analitical Mie solution (red-solid curve) for a Ag nanosphere of radius 5 nm. The 3D radiation pattern and two projections on the polarization plane and the propagation plane are plotted in (c) and (d), respectively. (e) Near electricfield intensity distribution in the polarization plane, (f) and NF intensity versus d/λ, distance from the surface normalized to the resonance wavelength, along the white line drawn in e) for the GTm (black-dashed curve) and Mie (red-solid curve).

larger: the charge is accumulated on the corners due to the fast variation of the curvature and that increases the scattered field. Secondly, the LSPR of the cube redshifts about 20 nm as we increase n. This can be understood upon taking into account that the SS changes from a surface close to a sphere ($n = 5$), to a cube ($n > 20$). Therefore the resonance wavelentgh has to evolve from a resonance close to that of a sphere with $r = 25$ nm, $\lambda \simeq 360$ nm, to the resonance of a sharp cube, at $\lambda \simeq 400$ nm. These two effects have been reported in Ref. [43], even though the method therein to round the cube is truncate its corners, which is very different to our approach. The SERS enhancement factor can be estimated from $|\mathbf{E}|^4$ evaluated on the surface. For the cubes under study we obtain a value from $|\mathbf{E}|^4 \sim 2 \cdot 10^4$, ($n = 8$) to $|\mathbf{E}|^4 \sim 9 \cdot 10^4$, ($n = 20$). Even though those values of the enhancement factor make single nanocubes suitable SERS substrates, they are not large enough to guarantee in general detectable SERS signals.

To illustrate the versatility of the method, we now study a complex nanoparticle with low symmetry such as a nanostar. The parameters of the SS for star shape are $1 > n_1 > 0,2 > n_2 = n_3 > 1,1 = b = 1, m \geq 3$, where m rules the symmetry of the star. In Fig. 4 the extinction cross section, the surface field distribution, and the far field pattern are shown for a 5-fold symmetry nanostar with only a symmetry axis, with parameters $n_1 = 0.2, n_2 = n_3 = 1.85, a = b = 1, m = 5$ for both realizations of the parameters of the SS, [$r_1 = r_2$ in Eq. (11)]. The incident field propagates along the z-axis from bottom to top, and the polarization is oriented along the x-axis (see Fig. 4). There is only a strong LSPR at $\lambda = 380$ nm, which exhibits very asymmetric radiation patterns, shown in the far field distribution, Fig. 4(c). (In [44] the plasmon resonances of 2D nanostars are calculated, which are essentially dipolar). The 3D nanostar reveals a richer,

#144976 - $15.00 USD Received 29 Mar 2011; revised 19 May 2011; accepted 22 May 2011; published 8 Jun 2011

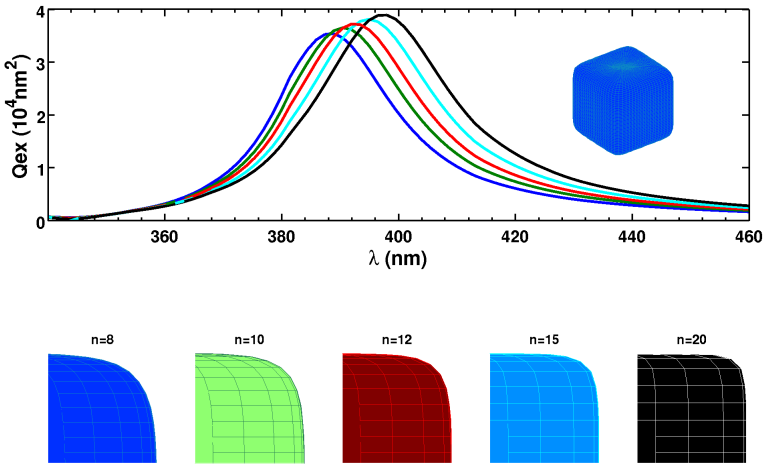

Fig. 3. Extinction cross sections for rounded Ag nanocubes with $L = 50$ nm with varying vertex sharpness: SS parameters $n_1 = n_2 = n_3 = n$, $a = b = 1$, $m = 4$, for both realizations ($r_1 = r_2$) of Eq. (11).

extremely asymmetric structure with many lobes. In spite of such asymmetry, note that in the plane of polarization, the far field distribution consists of two opposed lobes reminiscent of a dipolar pattern, with a much larger lobe directed along the forward direction, stemming from the top star spike (see Fig. 4(d)). The enhancement factor for the nanostar is $|\mathbf{E}|^4 \sim 10^7$, which is a value large enough to SERS applications as pointed out in [44]. To the best of our knowledge, this is the first time that a full calculation for the scattering of a 3D-star shape has been shown in the literature; the only attempt has been performed on a system with axial symmetry consisting of a sphere with two spikes [45].

4.3. Symmetric and asymmetric dimers

In Fig. 5, we show the scattering cross section of three sort of dimer: namely, sphere-sphere (*ss*), cube-cube (*cc*), and cube-sphere (*cs*). Dimers have been intensely used in Plasmonics and Nanophotonics due to the large fields generated in the gap, and their behaviour as optical nanoantennas [12, 42]. The scatterers are made of silver with $r = 15$ nm in the case of the sphere, and $L = 30$ nm in the case of the cubes, with the gap width $g = 1.5$ nm; in all cases the polarization of the incident field is along the dimer axis. Firstly, we have to point out the fact that the system ss can be compared to the extended Mie model [46]. The GTm reproduces both the position of the resonances and the shape of the spectra. By inspecting the three spectra, we can conclude that the spectrum of the system *cs* is a mixture of both the *ss* system and the *cc*, due to the fact the *cs* system shares features of both within the range $\lambda = 340 \sim 370$ nm. In addition, the main longitudinal LSPR at $\lambda = 405$ nm lies between those of the systems *ss* and *cc*. The same holds for the surface EM field intensity at the hot spots on the three systems, which explains the similarities between all of them. The SERS enhancement of those structures is about $|\mathbf{E}_{ss}|^4 \sim 4 \cdot 10^8$, $|\mathbf{E}_{cs}|^4 \sim 1 \cdot 10^{10}$, $|\mathbf{E}_{ss}|^4 \sim 10^9$, that reveals the incomparable features of those structures as SERS substrates.

#144976 - $15.00 USD Received 29 Mar 2011; revised 19 May 2011; accepted 22 May 2011; published 8 Jun 2011

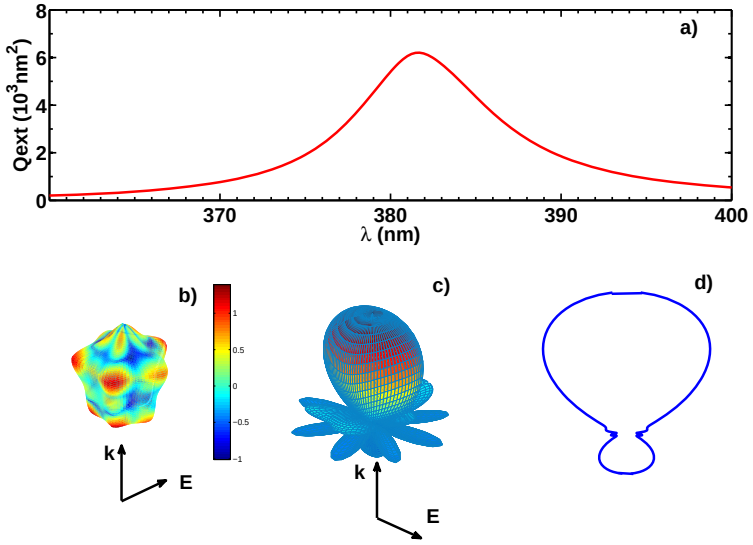

Fig. 4. (a) Extinction cross section for a 5-fold starlike silver nanostructure with SS parameters $n_1 = 0.2, n_2 = n_3 = n = 1.85, a = b = 1, m = 5$: thus the distance from center to the farthest tip is 50 nm. (b),(c) Surface electricfield distribution and 3D radiation pattern at the LSPR wavelength $\lambda = 365$ nm; the proyection of the radiation pattern on the polarization plane is shown in (d).

5. Conclusion

In this paper we have developed a numerical implementation in parametric coordinates based on the second Green's Theorem for the light scattering from nanoparticles called 3D-GTm. The surfaces have been described by equations called flexible surfaces, more specifically the one called *Supershape*. Both together the implementation of the 3D-GTm for an arbitrary number of three dimensional scatterers with different shape and electromagnetic properties, and surfaces without any specific symmetry as the flexible surfaces, become a powerful approach to scattering problems involving different kind of shapes, electromagnetic sources, materials on the scatterers and surrounding media. In addition, our method has three critical advantages. Firstly, the formalism is formally exact, so it takes into account the full non retarded multipolar contributions. Secondly, it needs a unique implementation to achieve a huge sort of different shapes. Thirdly, the numerical implementation scales with the particle surface rather than with its volume. Results are presented only for metal nanoparticles, but the formulation can be directly applied to dielectric scatterers, e.g. to tailor the magnetic response of Si nanoparticles [47]. Although the formulation introduced in this paper is restricted to isotropic dielectric permittivity, the GTm can be generalized to the study of dielectric nanoparticles with magneto-optical response. In order to show the validity and versatility of the method, we have studied different nanoparticles commonly used in experimental configuration of interest in Plasmonics and Nanophotonics: Spheres, cubes, stars, and dimers. We deal with complex isolated nanoparticles and interacting ones, including information about the cross sections, the radiation properties in order to understand the features of the plasmonic resonances, along with the surface and near field distributions at resonance wavelengths. For instance, the redshift of nanocube LSPR upon sharpening the corners is rigorously revealed. In addition, strong LSPR of 3D nanostars of inter-

#144976 - $15.00 USD Received 29 Mar 2011; revised 19 May 2011; accepted 22 May 2011; published 8 Jun 2011

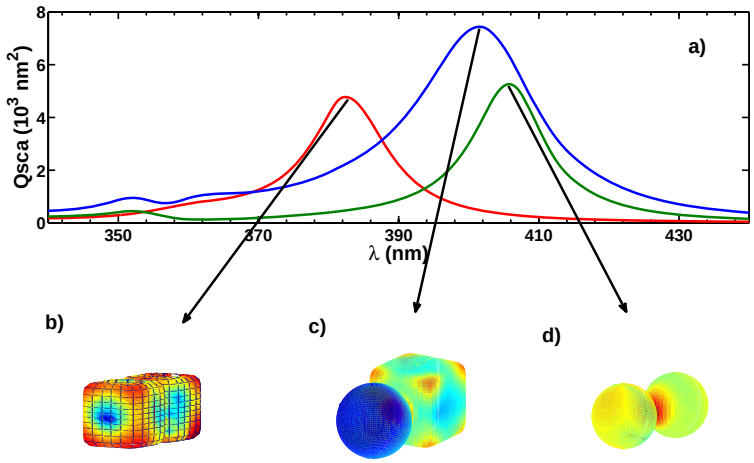

Fig. 5. (a) Scattering cross sections of three different kind of nanodimers. The incident field propagates normal to the cube sides with the polarization vector oriented along the axis of the dimers. In (b),(c) and (d) we show the intensity of the surface electric field distribution at the LSPR of the three systems studied: (b) cube-cube, (*cc*), (c) cube-sphere, (*cs*), (d) and sphere-sphere, (*ss*). Dimensions are: $L = 30$ nm (cubes), $r = 15$ nm (sphere), and gap$= 1.5$ nm.

est in SERS are shown to exhibit large field enhancements and extremely asymmetric radiation patterns. With regard to SERS, longitudinal LSPR of symmetric and asymmetric nanodimers are also investigated that yield larger enhancement factor within the gap region. The method that we have introduced along this article is fully applicable to a wide range of physics disciplines involving EM waves at different spectral regimes (optical, IR, THz,...), as metamaterials, nanophotonics, optical nanoantennas.

Acknowledgments

We are grateful to Demetrio Macías for bringing to our attention the superformula. The authors acknowledge support both from the Spain Ministerio de Ciencia e Innovación through the Consolider-Ingenio project EMET (CSD2008-00066) and NANOPLAS (FIS2009-11264), and from the Comunidad de Madrid (grant MICROSERES P2009/TIC-1476).

#144976 - $15.00 USD Received 29 Mar 2011; revised 19 May 2011; accepted 22 May 2011; published 8 Jun 2011